

Exploration of spatio-temporal distribution of aerosol and cloud properties over the Aral Sea Region using MODIS satellite data

Seminar on Cloud-Aerosol Interaction

Faculty of Geography, University of Marburg

Sarah Brüning

Darius A. Görgen

Lecturer

Dr. Boris Thies

Date

December 19, 2019

Number of words

4930

Contents

Contents	i
List of Figures	ii
1 Introduction	1
2 Data and Methods	3
2.1 Study area	3
2.2 Satellite products	4
2.2.1 Aerosol properties	4
2.2.2 Cloud properties	5
2.3 Methodology	6
3 Results	7
3.1 Temporal and spatial variations	7
3.2 Relationship between aerosol and cloud properties	17
4 Discussion	21
5 Conclusion	22
6 References	23
7 Appendix	27

List of Figures

1	Overview of the study domain within the ASB (Grey-scale values represent elevation, solid red lines national boundaries and dashed isolines average yearly sums of precipitation based on CHIRPS for the years 2003-2018).	4
2	Boxplots for yearly aerosol properties of AE (left), AOD (middle) and SSA (right).	9
3	Boxplots for monthly aerosol properties of AE (left), AOD (middle) and SSA (right).	10
4	Boxplots for yearly cloud properties of CER (left), COT (middle) and CWP (right).	11
5	Boxplots for monthly cloud properties of CER (left), COT (middle) and CWP (right).	12
6	Spatial distribution of seasonal means for AOD for spring (a), summer (b), autumn (c), and winter (d).	13
7	Spatial distribution of seasonal means for AE for spring (a), summer (b), autumn (c), and winter (d).	13
8	Spatial distribution of seasonal means for SSA for spring (a), summer (b), autumn (c), and winter (d).	14
9	Spatial distribution of seasonal means for COT for spring (a), summer (b), autumn (c), and winter (d).	15
10	Spatial distribution of seasonal means for CER [in microns] for spring (a), summer (b), autumn (c), and winter (d).	15
11	Spatial distribution of seasonal means for CWP [in g/m ²] for spring (a), summer (b), autumn (c), and winter (d).	16
12	Spatial distribution of correlation coefficient rho between AOD and AE during spring (a), summer (b), autumn (c), and winter (d).	18
13	Spatial distribution of correlation coefficient rho between AOD and SSA during spring (a), summer (b), autumn (c), and winter (d).	18
14	Spatial distribution of correlation coefficient rho between AOD and COT during spring (a), summer (b), autumn (c), and winter (d).	19
15	Spatial distribution of correlation coefficient rho between AOD and CER during spring (a), summer (b), autumn (c), and winter (d).	20
16	Spatial distribution of correlation coefficient rho between AOD and CWP during spring (a), summer (b), autumn (c), and winter (d).	20
17	Spatial distribution of linear trend for AOD during spring (a), summer (b), autumn (c), and winter (d).	27

18	Spatial distribution of linear trend for AE during spring (a), summer (b), autumn (c), and winter (d)	27
19	Spatial distribution of linear trend for SSA during spring (a), summer (b), autumn (c), and winter (d)	28
20	Spatial distribution of linear trend for COT during spring (a), summer (b), autumn (c), and winter (d)	28
21	Spatial distribution of linear trend for CER [in microns] during spring (a), summer (b), autumn (c), and winter (d)	29
22	Spatial distribution of linear trend for CWP [in g/m ²] during spring (a), summer (b), autumn (c), and winter (d)	29

1 Introduction

The desertification of the Aral Sea can be seen as one of the most prominent human induced natural disaster of the 21st century (Ge et al., 2016, p. 1; Groll et al., 2019, p. 1; Micklin, 2007; Shen et al., 2019, p. 1). With the aim of establishing cotton agriculture in the 1960's, an overexploitation of the sea's natural resources had begun and lead to an irreversible decrease in the water volume and the formation of a new desert in the former lake bed, the Aralkum (Gaynullaev et al., 2012, p. 1). This process is summarized under the term of the Aral Sea syndrome implying that the irrigation agriculture has not been proven to be adjusted to the local ecosystem's demands. Hence it can be seen nowadays as a first-class example of direct human influence in the natural surrounding (Groll et al., 2013, p. 1f). Coupled with severe environmental impacts comes a variety of ecological, economic and social challenges (Issanova et al., 2015, p. 3213ff). Added to that, the growth of the Aralkum leads to a rising dust storm frequency (Groll et al., 2013, p. 2). While mineral aerosols play a major role in the composition of these storms, climatological mechanisms of much higher complexity can be initiated (*ibid.*). One of these are the aerosol-cloud interactions which may affect local and regional climatology as well as the hydrological cycle (Boucher et al., 2013, p. 573ff.). As reliable results for their environmental effects are still lacking in the Aral Sea region, the present study will set out to identify trends in relationships between the aerosol composition and cloud microphysics (Rosenfeld et al., 2014, p. 750ff.).

The investigation of aerosol's influences on cloud microphysics has become a key topic of scientific research (Alam et al., 2010, p. 1162; Sharif et al., 2015, p. 657). There exist four major terrestrial sources for atmospheric aerosols: desert dust, biomass burning, biogenic and anthropogenic air pollution (Huang et al., 2014, p. 398). Based on their chemical composition, they either absorb or scatter incoming solar and terrestrial radiation which not only modifies the temperature profiles of the atmosphere directly but also develops indirect effects on the cloud lifetime, cloud albedo and precipitation formation (Sharif et al., 2015, p. 657f.). Aerosols can act as cloud condensation nuclei (CCN) leading to more and smaller droplets which increase the cloud albedo when a constant liquid water content is assumed (Costantino and Bréon, 2010, p. 1). This is called the first indirect aerosol effect or "Twomey effect". The second indirect effect ("Albrecht effect") relates to the hydrological cycle by prolonging the cloud's lifetime through the prevention of coalescence due to the increased number of droplets. Aerosols can suppress super-saturation within the clouds and thus lead to a reduction of precipitation rates (Boucher et al., 2013, p. 606ff.).

In the semi-arid and arid regions of Central Asia, absorbing desert dust aerosols play a significant role for climate forcing as well as for cloud and precipitation formation (Huang et al., 2014, p. 398f.). Studies

show that in Northern Africa and in parts of Central Asia mineral aerosols tend to inhibit precipitation (Rosenfeld et al., 2001, p. 5975). Over arid regions, they can even aggravate droughts through the effects of a feedback-loop as described by Huang et al. (2014): While a high aerosol concentration causes more CCN and an increased number of cloud droplets for the available water vapour in the atmosphere, the suppressed coalescence and subsequent decrease of rainfall lead to a diminished soil moisture which in turn causes more dust storms. As a result, the cloud cover and water vapour are decreased with an increasing aerosol concentration, leading to expanding desertification (Huang et al., 2014, p. 408f.).

In general, dust aerosols are relatively big particles with an Ångström Exponent (AE) smaller than 1 and a low single scattering albedo (SSA) (Huang et al., 2006, p. 1ff.; Moosmüller et al., 2012, p. 2f.). A number of studies showed the presence of a strong seasonality in regard to aerosol concentration in Central Asia (Ge et al., 2016, p. 62ff.; Li and Sokolik, 2018, p. 2ff.). The highest values occur in spring while the lowest concentrations have been measured in winter (*ibid.*). However, some studies also suggest the existence of spatial differences in the aerosol loadings next to patterns of temporal variability (Alam et al., 2010, p. 1163ff.). Furthermore, aerosol as well as cloud properties are said to follow a distinct seasonal cycle, which work in opposite directions underlining not only the temporal variability but also a possible connection between aerosols and cloud microphysics (Rosenfeld et al., 2014, p. 752ff.).

The goal of the study is to analyse spatial and temporal variations of aerosols in the Aral Sea region and their correlation to cloud microphysical parameters. The analysis consists of the investigation of potential trends, their strength and direction in regard to individual aerosol and cloud properties. By using proxy variables, namely AE and SSA, the dominating aerosol types and linked potential changes are narrowed down. Additionally, the study examines the relationship between aerosol and cloud properties which are discussed in the light of the theory of the first and second indirect aerosol effect. Based on the results of previous studies, MODIS time-series and correlation analyses are used to investigate the assumption that the aerosol concentration – described by the aerosol optical depth (AOD) - rose significantly in the time period 2003 - 2018 (Li and Sokolik, 2018, p. 1ff.). Others have shown a clear spatial and temporal pattern for aerosols with the highest values to be found in spring (Ge et al., 2016, p. 62ff.) as well as in the northern and central regions of the Aral Sea (Li and Sokolik, 2018, p. 2f.). There is some evidence of increasing particle sizes pictured by a decrease in AE over the course of time (Sharif et al., 2015, p. 658f.). Based on the chemical composition of dust aerosols seems to follow a decrease in SSA resulting in higher absorption of radiation (Huang et al., 2014, p. 408ff.). For other regions it has been shown that a stronger aerosol concentration and consequently increased CCN lead to a distinct cloud albedo and density (COT) while the cloud droplet size (CER) is reduced (Alam et al., 2010, p. 1163). Thus, AOD and CER have an opposed diurnal variation,

while it is likewise for AOD and COT or CWP (Rosenfeld et al., 2014, p. 752ff.). On the other hand, the liquid water content (CWP) can be enhanced through a higher amount of available water in the cloud. These assumptions help in presuming the presence of the first and second indirect effect (Yin et al., 2002). In contrast to these effects, a negative relationship between the AOD, the CER and the CWP can emphasize the existence of a precipitation feedback-loop (Huang et al., 2014, p. 408ff.). This said, the result of the following analysis remains to be seen.

2 Data and Methods

2.1 Study area

The Aral Sea basin is located in the border region between Kazakhstan and Uzbekistan ($57 - 67^{\circ}\text{E}$, $42 - 49^{\circ}\text{N}$) and acts as the tail-end lake of the contributing rivers Amu Darya and Syr Darya (Figure 1). The study area is part of the global dust belt and shows typical features of a temperate continental climate with semi-arid to arid conditions. The summers are short and hot with a mean of 28.2°C while winters are long and cold with a mean of -3.6°C . Precipitation rates are quite low with a mean of about 82.1 mm/year and a maximum during winter (Gaynullaev et al., 2012, p. 287). Strong winds are often to be recorded in the study area (Issanova et al., 2015, p. 3213f.). The Aral Sea once has been the fourth largest lake on earth covering a water volume of 1.093 km^3 in 1960 (Gaynullaev et al., 2012, p. 286). Since then, it has been gradually shrinking due to overexploitation of its natural resources by water abstraction for irrigation agriculture as well as the impacts of climate change (Ge et al., 2016, p. 2; Shen et al., 2019, p. 2031). In the year 2003, it finally split into eastern and western parts. The exposed lake bed consists of salt soils and loose sand dunes turning the former southern and western part of the lake into the Aralkum desert (Shen et al., 2019, p. 2031f., 2016, p. 624) which comprises of 57.500 km^2 (Opp et al., 2019, p. 3). The landscape is characterized by frequent salt and sand dust storms which may bear several threats to the ecosystem and local human's health (Ge et al., 2016, p. 4). It has been stated that the spatial and temporal dust deposition variability is highly significant (Opp et al., 2019, p. 1ff.).

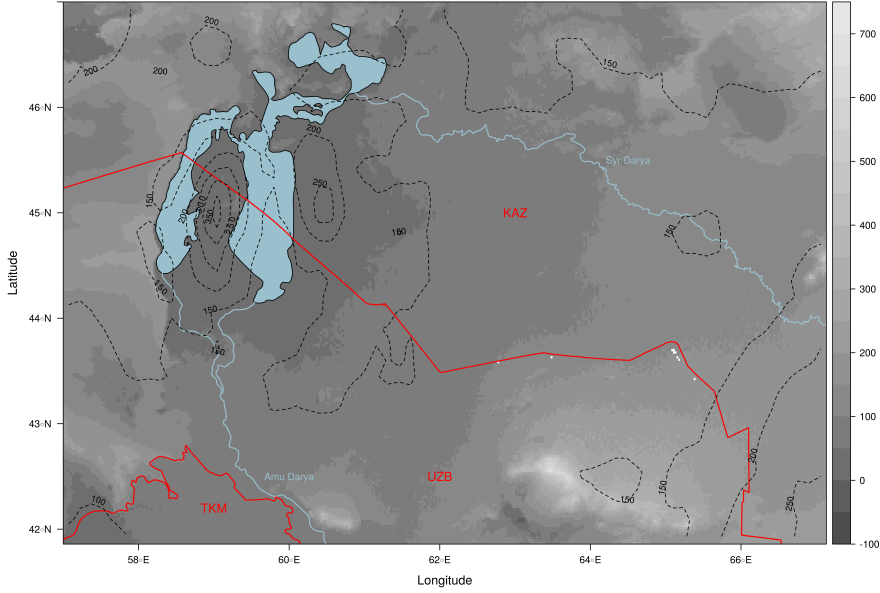


Figure 1: Overview of the study domain within the ASB (Grey-scale values represent elevation, solid red lines national boundaries and dashed isolines average yearly sums of precipitation based on CHIRPS for the years 2003-2018).

2.2 Satellite products

MODIS (Moderate Resolution Imaging Spectroradiometer) data currently is collected by two platforms (TERRA and AQUA) orbiting the Earth on a Sun-synchronous polar orbit. It measures solar and thermal radiation in 36 bands in resolutions ranging from 250 m to 1 km . For this study, daily resolution Level-2 data were used for aerosol (MOD/MYD04) (Levy et al., 2017) and cloud (MOD/MYD06) (Platnick et al., 2017) parameters as well as the corresponding geolocation files (MOD/MYD03) (*MODIS Geolocation Fields 5-Min L1A Swath 1km V006*, 2012).

2.2.1 Aerosol properties

The aerosol parameters AOD, AE and SSA were retrieved based on the Deep Blue algorithm (DB) described by Hsu et al. (2004) and Hsu et al. (2006). DB uses wavelengths in the blue spectrum to overcome the phenomenon of absorbing aerosols darkening the reflectance measured at the sensor over bright surfaces making it more suitable for aerosol retrievals over bright surfaces such as deserts (Hsu et al., 2004). It is applied to clear-sky snow-free pixels over land only and uses the 412, 470/490, 650, 860, 1240 and $2110\text{ }\mu\text{m}$ spectral bands on a final pixel size of $10 \times 10\text{ km}$ (Hsu et al., 2013).

Ångström Exponent (AE): AE is a wavelength depended parameter which is widely used as a qualitative measure of the particle size distribution of aerosols (Floutsi et al., 2019; Kang et al., 2015; Li and Sokolik, 2018; Rupakheti et al., 2019; Soni et al., 2011; Yin et al., 2016). It is inversely related to particle size with values ≤ 1 indicating a dominating coarse-mode of aerosols and values > 1 indicating the dominance of fine-mode aerosols (Soni et al., 2011). Depended on the wavelength the Angstrom exponent α is calculated according to Formula 1:

$$\tau_a(\lambda) = \beta(\lambda) - \alpha \quad (1)$$

with: τ_a : AOD λ : wavelength α : AE

In the MOD04 product α is calculated on the basis of the 412 and 470 μm bands with the DB algorithm.

Aerosol Optical Depth (AOD) and Single Scattering Albedo (SSA): The calculation of AOD and SSA is based on established lookup tables which are differentiated for several regions around the globe based on dominant aerosol modes found by empirical measurements (Hsu et al., 2004). Two different retrieval techniques can be applied: For moderate dust loadings with $AOD < 0.7$ the algorithm uses a two-channel technique to retrieve aerosol parameters based at 412 and 470/490 μm . Under heavy dust loadings with $AOD > 0.7$ a three-channel technique with the additional 670 μm band may retrieve values for the combination 412 vs. 670 μm and 470/490 vs. 670 μm .

2.2.2 Cloud properties

The algorithm to retrieve cloud optical and microphysical parameters at a nominal resolution of 1 km makes use of the 645, 1640, 2130 and 3750 μm channels over land during daytime. It is applied to cloud overcast pixels only and differentiates the calculation according to the dominant phase of the cloud (Baum et al., 2012). Additionally, information of the surface albedo is included in the algorithm since cloud reflectance is altered due to the underlying surface characteristics. Here, only the parameters describing the cloud's microphysics (COT, CER and CWP) are extracted.

Cloud Effective Radius (CER) and Cloud Optical Thickness (COT): CER and COT are derived from water-absorbing bands of MODIS (1.6, 2.1, 3.7 μm) coupled with non-absorbing bands (0.65, 0.86 and 1.2 μm) (Platnick et al., 2003). The algorithm uses a radiative transfer model to calculate a reflected intensity field for combinations of CER and COT. Both parameters are then retrieved based on the measured reflectance. With the introduction of the algorithm version C6 the retrieval of cloud parameters for optical thin clouds has been enabled (Platnick et al., 2017). For this study the data layers which retrieve CER and COT based

on the relation between $2.1 \mu\text{m}$ and 0.65 , 0.86 and $1.2 \mu\text{m}$ were used.

Cloud Water Path (CWP): The CWP is directly linked to CER and COT and refers to the total liquid water amount found in the atmospheric column above a given pixel. It can be calculated in a simplified manner by use of Formula 2:

$$CWP = y * CER * COT \quad (2)$$

This form of the calculation is beneficial for satellite-based measurements, since CWP can be estimated with information on COT and CER only. The term y is either determined by adiabatic assumptions (Wood, 2006) or the assumption of a vertically homogeneous water column (Stephens et al., 1978) becoming either the ratio $5/9$ or $2/3$, respectively.

2.3 Methodology

The parameters are extracted from the MODIS data using the HEG-Tool (HDF-EOS To GeoTIFF Conversion Tool). It enables a selection of the cloud and aerosol properties clipping the data directly to the area of interest which is leaned on the shape of the study area used by (Ge et al., 2016). After aggregating the daily data to a monthly resolution, means for every season are calculated in order to detect inter-annual variability and linear trends. For each parameter, the long-term temporal dynamic between 2003 - 2018 is analysed as well as the seasonal variability by using boxplots of monthly and yearly mean values (Li and Sokolik, 2018, p. 12). The statistical analysis includes the trend detection to reveal the existence as well as the strength and direction of a possible change based on a seasonal resolution (Spring: March, April, May; Summer: June, July, August; Autumn: September, October, November; Winter: December, January, February). For analysing the time series, the robust and non-parametric approach introduced by the Mann-Kendall test is used (Li and Sokolik, 2018, p. 16). This test is suitable for non-normal distributed data and therefore applicable for environmental data (Kendall, 1975, p. 55ff.). As the Mann-Kendall test only provides information on the existence of a trend, its strength and direction are analysed using a simple linear regression (Li et al., 2014, p. 12273ff.). The trend's direction can be evaluated by the sign and the strength of its distance from 0. It is applied on a pixel basis for each season in order to detect spatial as well as temporal differences (Alam et al., 2010, p. 1164ff.). The relationship between the cloud and aerosol parameters is investigated through correlation tests (Sharif et al., 2015, p. 657ff.). Due to the missing conditions for using the Pearson correlation coefficient the method by Spearman is applied. The correlation coefficient is available in a standardised

format between -1 and 1, with values at the end of the scale indicating a nearly perfect correlation (Spearman, 1987, p. 72ff.). The results of this analysis are presented on a pixel basis for each season to display spatial and temporal differences. Additionally, the correlation of all pixels is calculated to investigate the overall direction and strength of correlation between aerosol and cloud parameters (Alam et al., 2010, p. 1170f.).

3 Results

3.1 Temporal and spatial variations

The depicted time period shows the long-term changes of the aerosol and cloud parameters from 2003-2018. The AOD pictures a yearly mean value between 0.1 – 0.3 which at first increases until 2012 but decreases to the level of 2003 afterwards (Figure 2). Also, the data show a high standard deviation with many outliers, especially for values of $AOD > 0.5$. In contrast, the course of the AE values is higher deviating with a mean between 1.1 – 1.3. While the AOD reaches its maximum values in 2012, the AE decreases from 2003 – 2011. Afterwards it slowly increases to a similar level as in the first year of the study period. The quantiles include a larger value range for the AE than the AOD while their standard deviation is less distinct. Both parameters do not show a monotonous trend. In contrast, for the SSA, a constant decrease over the course of the time period can be observed. In 2003, the mean of the SSA is at 0.93, while in 2018 it drops below 0.91. The standard deviation is broad throughout the study period (*ibid.*). The analysis of the monthly means pictures a distinct seasonal cycle for AOD, where values seem to be typically higher in spring and autumn than in summer and winter (Figure 3). Opposing the seasonal dynamic of AOD, the AE reaches its maximum in summer and winter. Spring and autumn are characterized by lower mean values. The SSA shows lower values from January to June with moderately increased values from July to December (*ibid.*).

Concerning the long-term variations of the cloud properties, the values of all parameters show a high level of inter-annual variation in the depicted time period (Figure 4). The value range remains fairly constant for the entire period. COT and CWP show a very similar pattern of inter-annual variation, both reaching their highest mean value in 2009 (*ibid.*). CER values mostly range between 20 and 24 microns with a maximum in 2008, while COT values vary between 15 – 24 and CWP values between 150-240 g/m^2 . The analysis of the annual variability implies a more distinct seasonal pattern for COT and CER (Figure 5). In the transition seasons, COT reaches lower values than in summer and winter. In spring and summer, higher values lead to an expanded value span and standard deviation. The values of CER show an opposite seasonal cycle with the maximum in spring and autumn as well as the minimum in summer and winter. For CWP, a seasonal

cycle is not as distinct since the values show a typical distribution but without a clear seasonal pattern. In general, lower values go along with a smaller value range and vice versa (*ibid.*).

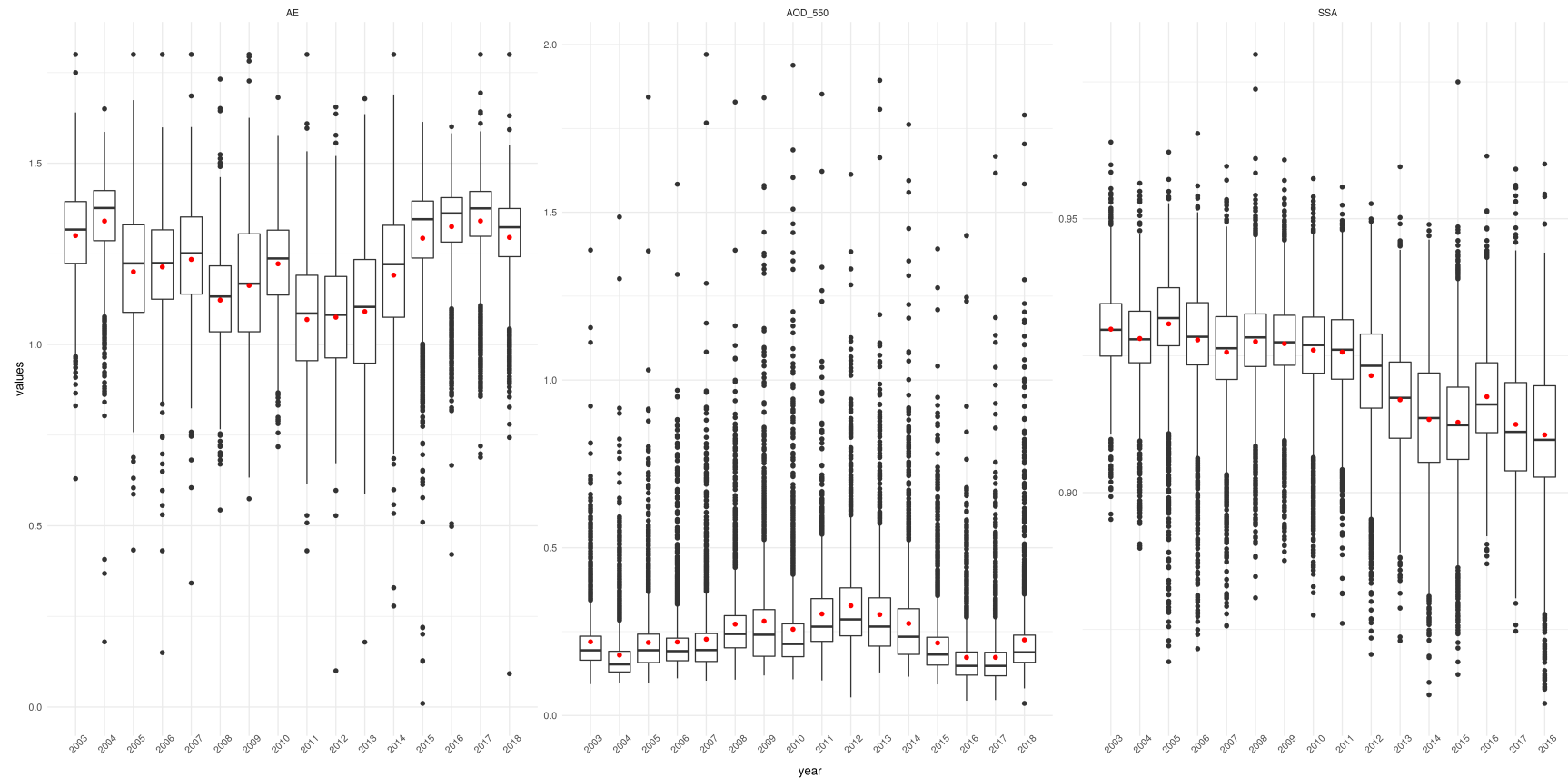


Figure 2: Boxplots for yearly aerosol properties of AE (left), AOD (middle) and SSA (right).

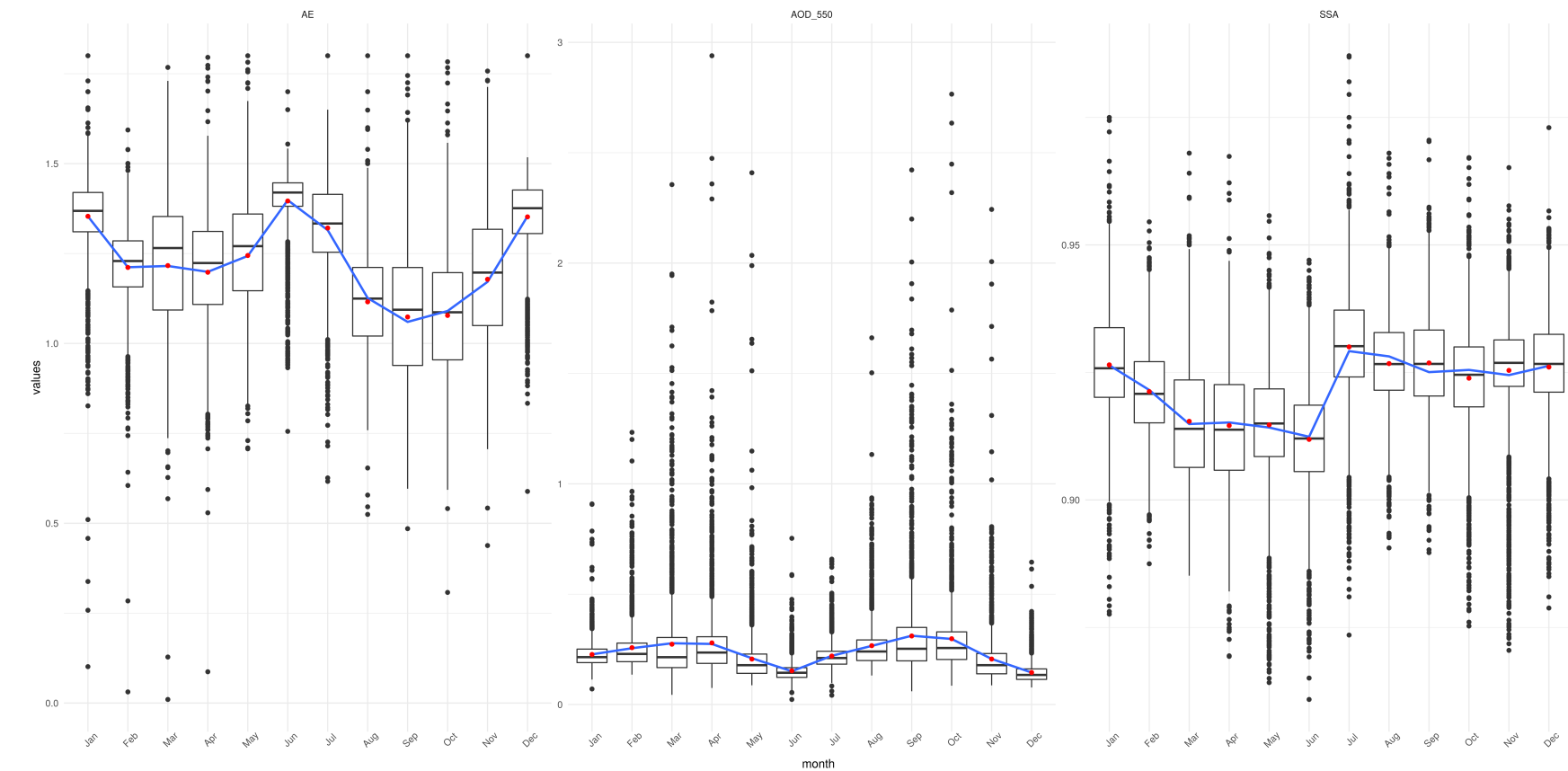


Figure 3: Boxplots for monthly aerosol properties of AE (left), AOD (middle) and SSA (right).

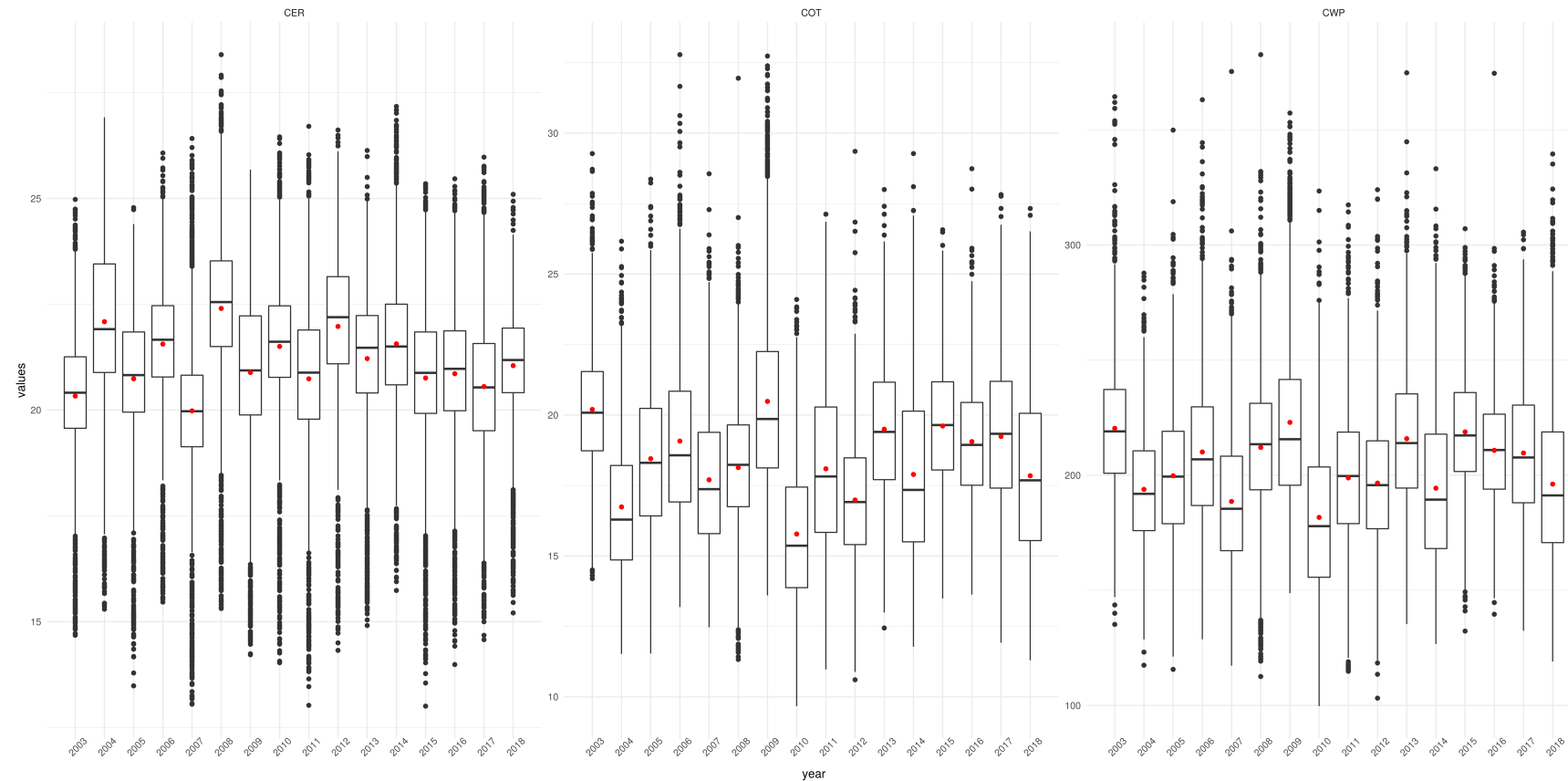


Figure 4: Boxplots for yearly cloud properties of CER (left), COT (middle) and CWP (right).

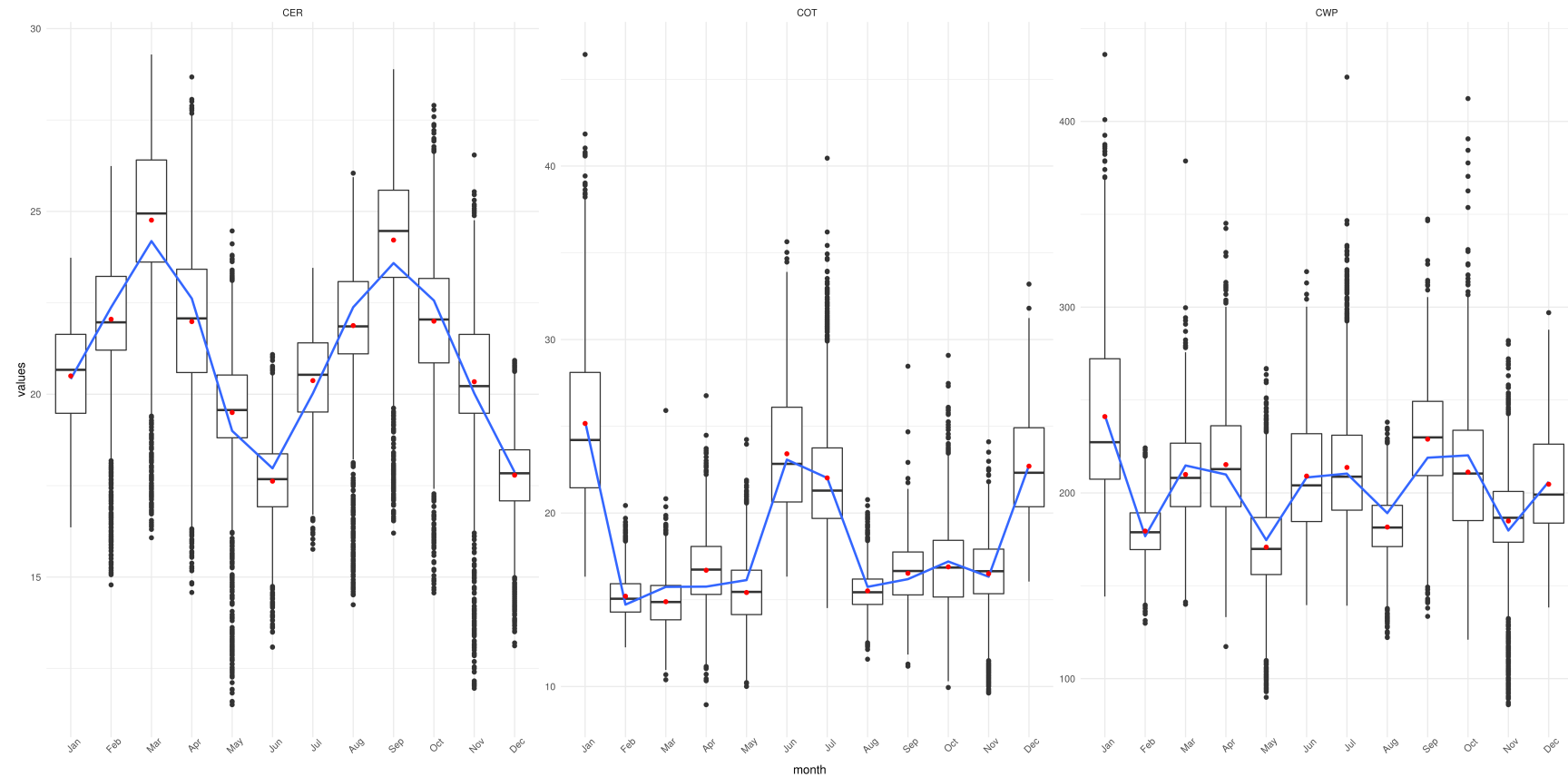


Figure 5: Boxplots for monthly cloud properties of CER (left), COT (middle) and CWP (right).

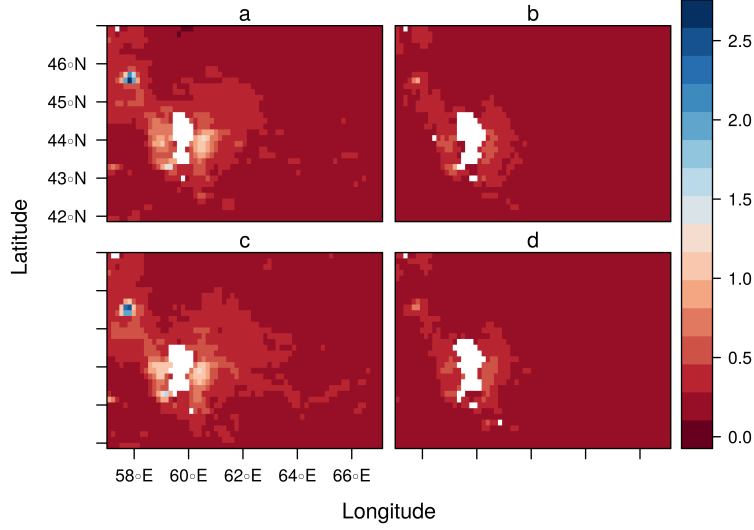


Figure 6: Spatial distribution of seasonal means for AOD for spring (a), summer (b), autumn (c), and winter (d).

Aerosol properties trend detection: The AOD is higher around and North-West of the Aral Sea with maximum values in spring and autumn (Figure 6). The long-term trend analysis shows an increasing trend close to the Aral Sea and Aralkum, while the values further away tend to decrease (Appendix, Figure 17). The slopes picture a rather small change for the mean values.

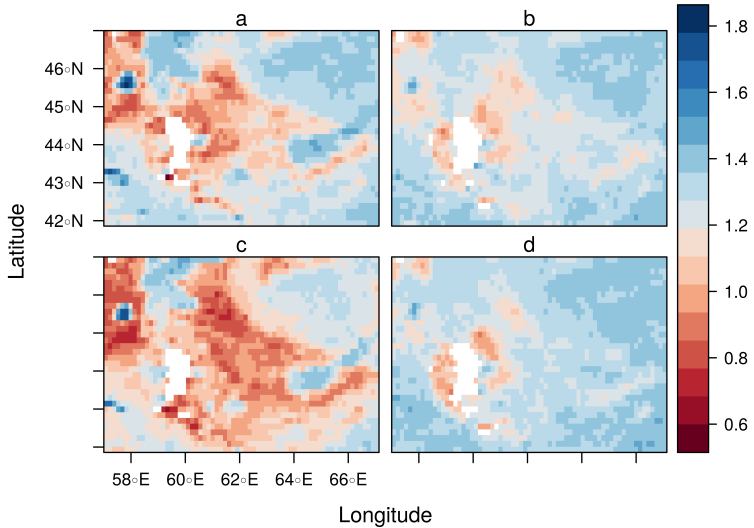


Figure 7: Spatial distribution of seasonal means for AE for spring (a), summer (b), autumn (c), and winter (d).

Contrary to this, the AE reaches its lowest values in spring and autumn, while the maximum appears in summer and winter (Figure 7). Overall, the AE increases with rising distance to Aral Sea. In spring and autumn, a great proportion of the areas East and West to the Aralkum show values of $\text{AE} < 1.0$. The trend detection depicts in spring, summer and winter mostly increasing values (Appendix, Figure 18). Only individual pixels show a significant increase especially in the East of the Aral Sea. In autumn, decreasing trends are dominating, but still can only be applied to the areas close to the lake surface and the Aralkum.

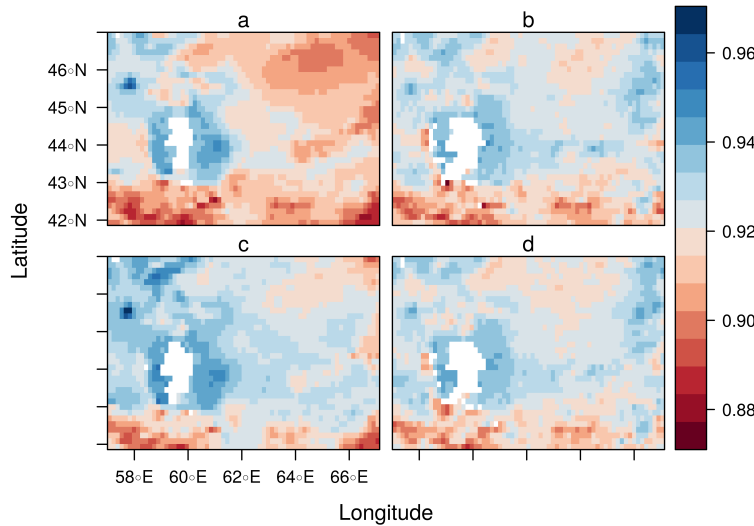


Figure 8: Spatial distribution of seasonal means for SSA for spring (a), summer (b), autumn (c), and winter (d).

The SSA shows a considerable spatial pattern with higher values around the Aral Sea (Figure 8). In the South and North-East of the study area, values are considerably lower. Especially in spring, there is a high variation between the individual regions. As for the trend detection, mostly decreasing trends are observed except for the spring season (Appendix, Figure 19). Close to the surface of the Aral Sea and the Aralkum, however, stronger increases in SSA are found during spring and autumn and fewer steep decreases in summer and winter. In contrast to the other aerosol properties, most of the pixels are characterized by a significant detection of a linear decreasing long-term trend. In contrast, a monotonous trend detection for AOD and AE is not possible on a whole scale level. Here, significant trends only appear for individual pixels with a high spatial and temporal divergence. In addition, all slopes only display slight changes as the slopes are weakly defined.

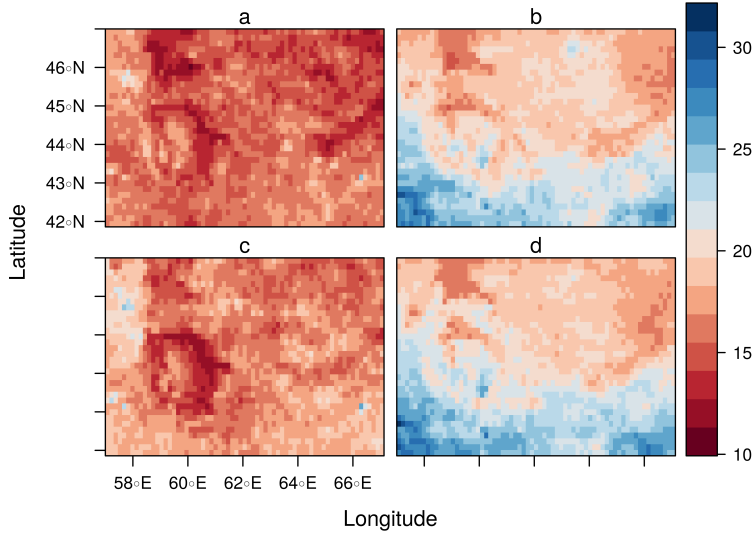


Figure 9: Spatial distribution of seasonal means for COT for spring (a), summer (b), autumn (c), and winter (d).

Cloud properties trend detection: The COT depicts a seasonal cycle with lowest values in spring and autumn and higher values in summer and winter (Figure 9). During the latter ones, maximum values are reached in the southern region. The Aral Sea and the Aralkum are visible as regions with moderately lower values. The trend analysis shows the dominance of positive slopes in spring and autumn especially around the Aral Sea and Aralkum whereas values in the other seasons are rather decreasing (Appendix, Figure 20).

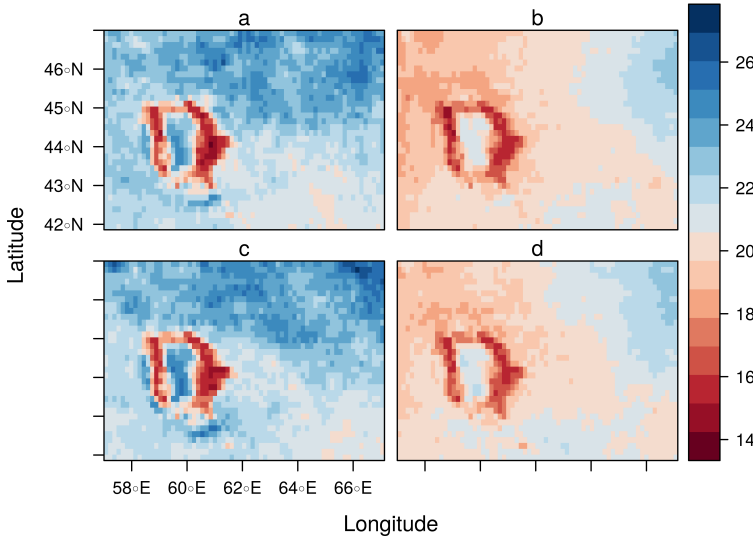


Figure 10: Spatial distribution of seasonal means for CER [in microns] for spring (a), summer (b), autumn (c), and winter (d).

Also, these regions are shown as well as a clear shape in all seasons for CER (Figure 10). They are characterized by very low values in contrast to the rest of the study area. Apart from that, values are generally higher in spring and autumn with the spatial maximum appearing in the North-East of the study area, while throughout all seasons lower values can be observed South-East and West of the Aral Sea's surface. The trend analysis agrees with the pattern of a decreasing CER during spring, autumn and winter especially around the lake and the Aralkum (Appendix, Figure 21).

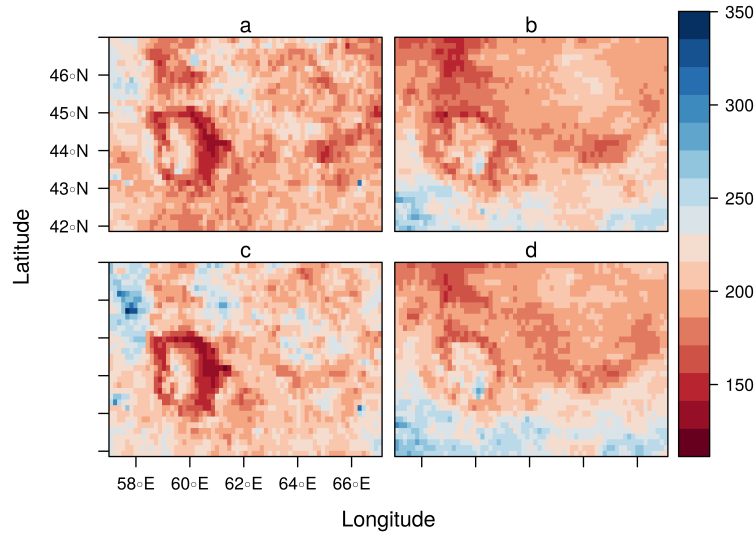


Figure 11: Spatial distribution of seasonal means for CWP [in g/m²] for spring (a), summer (b), autumn (c), and winter (d).

Minimal values for CWP during all seasons are observed around the Aral Sea as well while they increase only in the South of the study area during summer and winter (Figure 11). No clear seasonal differences are observed, instead, a diverging seasonal pattern dominates (Appendix, Figure 22). During spring and autumn, there is a very diverse pattern of trends. The slopes are positive during summer and winter in close distance to the lake and the Aralkum. These pixels are the only ones showing a significant trend during these seasons, but the rest of the study area is otherwise characterized by a decreasing CWP. Like for the aerosol properties, a linear trend detection for all cloud properties on a whole scale level is not possible. Individual parameters imply the existence of a trend, but most pixels do not apply to the significance level.

3.2 Relationship between aerosol and cloud properties

Relationship between aerosol properties: The analysis of the relationship between AOD and AE shows a seasonal dependence with mainly a moderate to high negative correlation (Table 1). The spatial analysis implies mostly negative values for the study area with the strongest relationship in the central region. They tend to be generally stronger in spring and autumn.

Close to the Aral Sea, there are some pixels showing a positive correlation, but only negative correlated pixels can be seen as statistically significant (Figure 12). The relationship between the AOD and SSA depicts an opposing and also weaker relationship, with more positive correlations and a higher spatial diversity (Table 1). However, again only negative correlations are found to be statistically significant especially during summer and autumn (Figure 13).

Table 1: Correlation coefficients between aerosol and cloud parameters by season.

parameters	spring	summer	autumn	winter
AE vs. SSA	-0.54	-0.11	-0.24	-0.23
AE vs. AOD	-0.77	-0.64	-0.77	-0.65
SSA vs. AOD	0.52	0.11	0.34	0.22
AOD vs. CER	-0.2	-0.15	-0.2	-0.1
AOD vs. CWP	0	-0.11	-0.08	-0.07
AOD vs. COT	0.08	-0.06	-0.04	-0.05

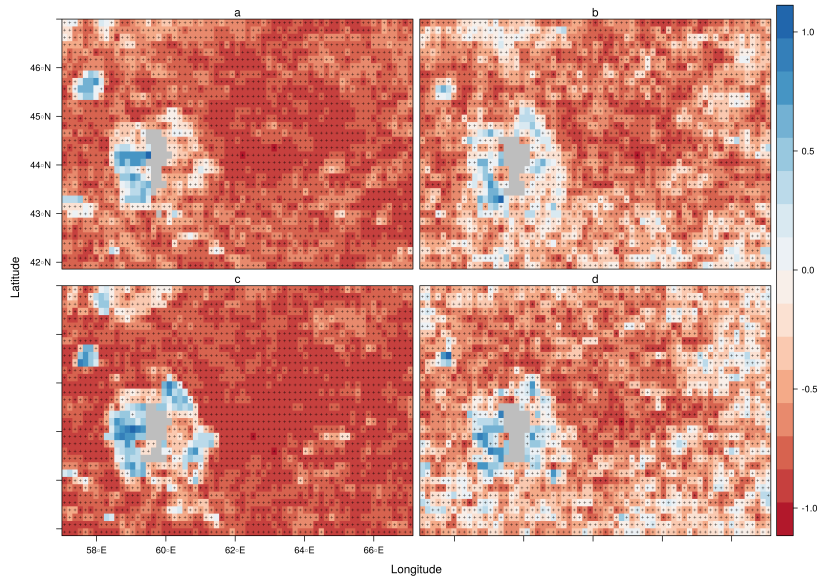


Figure 12: Spatial distribution of correlation coefficient rho between AOD and AE during spring (a), summer (b), autumn (c), and winter (d).

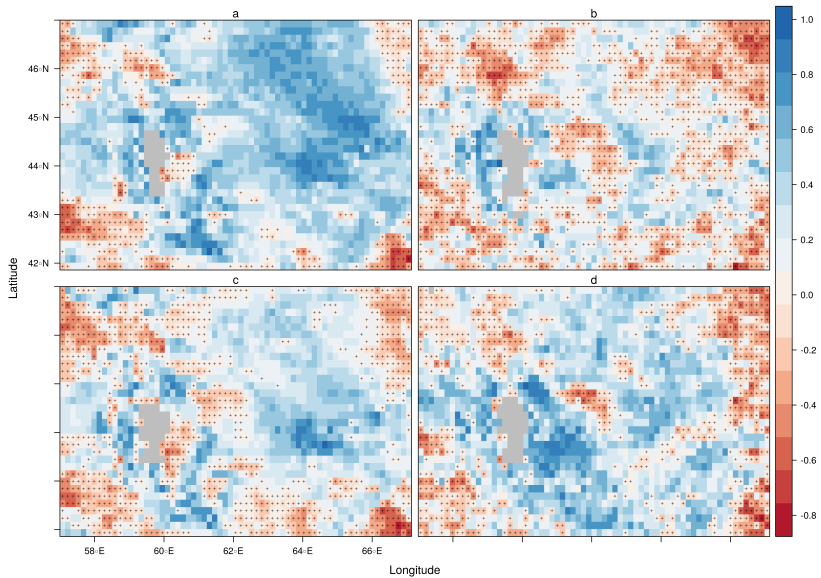


Figure 13: Spatial distribution of correlation coefficient rho between AOD and SSA during spring (a), summer (b), autumn (c), and winter (d).

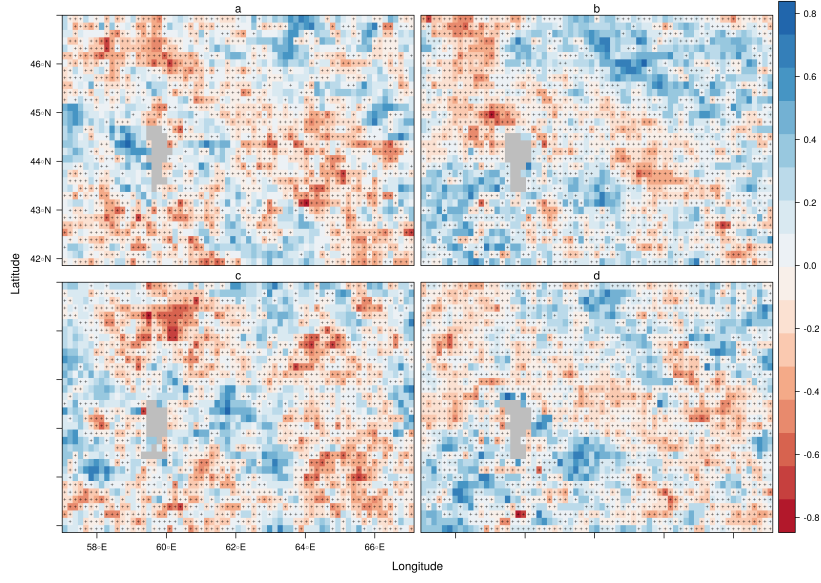


Figure 14: Spatial distribution of correlation coefficient rho between AOD and COT during spring (a), summer (b), autumn (c), and winter (d).

Relationship between AOD and COT: The relationship between AOD and COT shows overall very low to low correlation coefficients (Table 1). Based on this a highly mixed distribution of negative and positive correlation coefficients can be identified. The variation makes it hard to find a clear pattern, though there is a band of significant negative correlations from the North-West to the South-East of the study area. Most pixels showing a negative sign are statistically significant, even though the overall strength of the relationship is questionable (Figure 14).

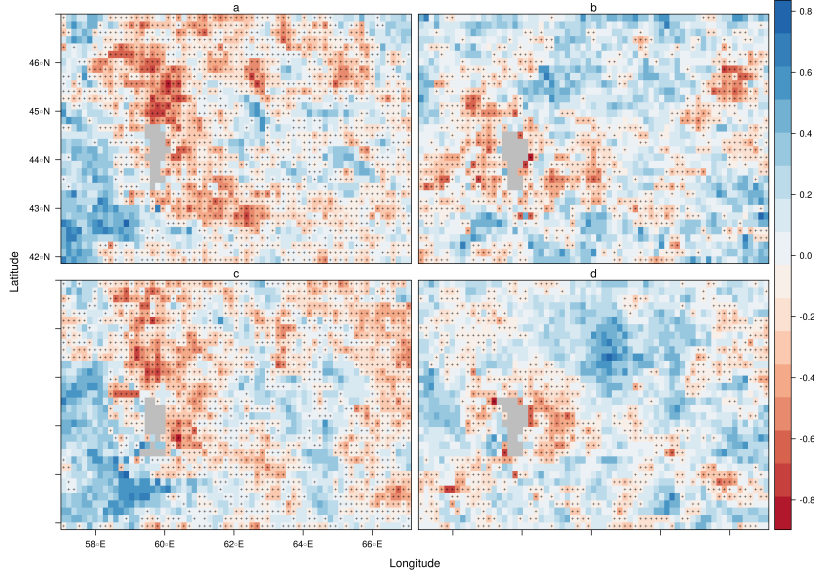


Figure 15: Spatial distribution of correlation coefficient rho between AOD and CER during spring (a), summer (b), autumn (c), and winter (d).

Relationship between AOD and CER: The AOD and the CER have a generally low to medium negative correlation (Table 1). The spatial analysis shows only negative correlations to be statistically significant. They tend to occur mostly in the central region of the study area as well as North and East of the Aral Sea and the Aralkum (Figure 15). The strongest relationship is observed during in spring and autumn (ibid.).

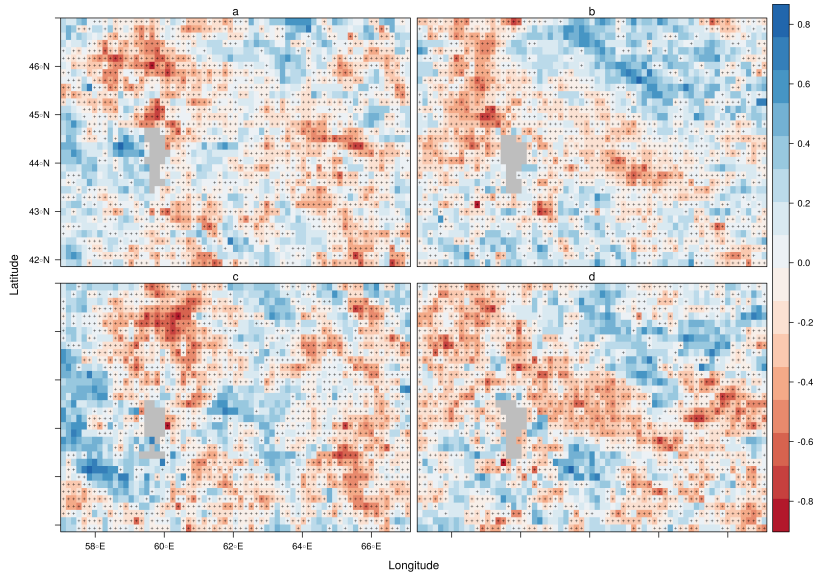


Figure 16: Spatial distribution of correlation coefficient rho between AOD and CWP during spring (a), summer (b), autumn (c), and winter (d).

Relationship between AOD and CWP: The relationship between AOD and the CWP is negative in total, with positive values only in spring. All values indicate a very low to low correlation (Table 1). The correlation maps show spatial highly deviating relationships with the highest values to be found North and West of the Aral Sea (Figure 16). Instead of a seasonal cycle, again a spatial pattern with a band of negative slopes on a highly significant level can be observed. Positive slopes rarely show significance throughout all seasons.

4 Discussion

Most of the depicted parameters do not show a monotonous trend. Contrary to former assumptions, the aerosol concentration does not show a linear increase from 2003 – 2018. While the size distribution reveals deviating values for AE, this proxy cannot be uniformly applied for estimating the aerosol type (Huang et al., 2014, p. 400ff.). Only in spring and autumn and together with an increasing absorption rate through decreasing SSA the hypotheses of dominating mineral dust is supported in some parts of the study area. For the cloud properties, no monotonous trend is visible. It is indicated that COT, CER and CWP are decreasing, but the statistical significance of these results is uncertain. Therefore, an analysis of the clouds microphysics is difficult. Also, the seasonal cycles which were assumed to fit together with the supposed relationships between aerosol and cloud properties do not overlap. Instead, the relationships between the individual parameters display rather weak correlations. In contrast to other studies in similar regions of Central Asia which obtained stronger results, their information value needs to be reconsidered (Alam et al., 2010, p. 1165ff.; Sharif et al., 2015, p. 660ff.).

In addition, the first and second indirect aerosol effect were analysed. Together with a rising AOD, a lower CER and an increasing COT, the Twomey effect may be assumed (Huang et al., 2014, p. 406ff.). The existence of the second indirect effect was investigated inspecting the correlation between AOD and CWP (*ibid.*). For small parts of the region – especially around the Aralkum – these hypotheses seem to be applicable. There are hints for a precipitation feedback loop because of the overall negative correlation between AOD and the cloud properties. But since the data show a tremendous variability in parameter's relationships and overall mostly low correlations, no definite statement for answering the scientific question is possible. The hypotheses set before can be neither confirmed nor denied. The analysis illustrates the complexity and difficulty of aerosol-cloud interactions as most relationships cannot be explained by merely the correlation coefficients used in this study. As pictured before, the aerosol cloud interactions demonstrate a high spatial and temporal variability with generally stronger characteristics in spring and autumn. Since all results cannot be confirmed for the whole study area and every parameter, they need to be treated with caution.

Instead, the influence of other parameters becomes apparent. These include not only meteorological conditions (Sharif et al., 2015, p. 657), but also the importance of external effects (Huang et al., 2006, p. 4). Mesoscale convective systems may cover local processes and can disguise the origin of interacting factors (Sharif et al., 2015, p. 660ff.). As no trajectory analysis is included, the origin of the aerosols stays unknown (*ibid.*). Furthermore, changes in the land use, e.g. through irrigation, may lead to more greening and less aerosol deposition, thus modifying the correlation results (Jin et al., 2017, p. 2f.). Also, the vertical structure of the clouds is an important feature in order to analyse the effects of aerosols on their hydrological cycle. Regarding these, the analysis needs to include more precise parameters to ensure reliable results (Costantino and Bréon, 2010, p. 4f.; Li and Sokolik, 2018, p. 22ff.). Apart from that the aggregation of the data can lead to an over- or underestimation of the estimated effects (Sayer et al., 2013, p. 7864ff.). In addition, the dimension of the existing retrieval bias in the MODIS data caused by the water surface of the Aral Sea stays unknown thus not leading to strictest results (Jin et al., 2017, p. 9f.). Nevertheless, there seems to be potential for optimizing (Li and Sokolik, 2018, p. 22ff.). The combination of instrumental and spatial difficulties inhibits a more detailed statement in regard to answering the scientific questions and hypotheses assumed before. This said, it is necessary to include a variety of possible influences in the analysis as well as taking further investigations in the cloud microphysical properties. Future research needs to take a closer look at the changes in the hydrological cycle: the feedback loop for rainfall rates may be implied, but its dimension and quantification in the region remain unclear.

5 Conclusion

As a result, the quantification of the aerosol-cloud interaction in the Aral Sea region includes several difficulties in gaining a reliable output. An accurate answer for the scientific questions needs to be replaced by a first approximation. The existence of a relationship between most of the aerosol and cloud properties can be assumed, but their strength, direction and possible consequences need to be further investigated. The results of this study may provide an overview for a study area that has not been object of this kind of research before. The problems that occurred can be led back to either instrumental and methodical issues or the complexity of natural processes. As the study itself dealt with a highly relevant topic many uncertainties in dealing with cloud microphysics still exist to this point. It is a future challenge to pursue solutions to these obstacles. Especially in highly vulnerable regions like the Aral Sea, changes in the hydrological pattern originating to aerosol concentration alterations may inhabit considerable threats to humans and nature, e.g. the expansion of deserts and ongoing salinization. Therefore, an estimation of precipitation patterns and shifts as well as

the clouds vertical structure and more precise aerosol type analyses are crucial for future research.

6 References

- Alam, K., Iqbal, M.J., Blaschke, T., Qureshi, S., Khan, G., 2010. Monitoring spatio-temporal variations in aerosols and aerosol-cloud interactions over Pakistan using MODIS data. *Advances in Space Research* 46, 1162–1176. <https://doi.org/10.1016/j.asr.2010.06.025>
- Baum, B.A., Menzel, W.P., Frey, R.A., Tobin, D.C., Holz, R.E., Ackerman, S.A., Heidinger, A.K., Yang, P., 2012. MODIS Cloud-Top Property Refinements for Collection 6. *Journal of Applied Meteorology and Climatology* 51, 1145–1163. <https://doi.org/10.1175/JAMC-D-11-0203.1>
- Boucher, O., Randall, D., Artaxo, P., Bretherton, C., Feingold, G., Forster, P., Kerminen, V.-M., Kondo, Y., Liao, H., Lohmann, U., Rasch, P., Satheesh, S., Sherwood, S., Stevens, B., Zhang, X., 2013. Clouds and Aerosols, in: Stocker, T., Qin, D., Plattner, G.-K., Tignor, M., Allen, S., Boschung, J., Nauels, A., Xia, Y., Bex, V., Midgley, P. (Eds.), *Climate Change 2013: The Physical Science Basis. Contribution of Working Group I to the Fifth Assessment Report of the Intergovernmental Panel on Climate Change*. Cambridge University Press, Cambridge, United Kingdom; New York, NY, USA., pp. 465–657. <https://doi.org/10.1017/CBO9781107415324.015>
- Costantino, L., Bréon, F.M., 2010. Analysis of aerosol-cloud interaction from multi-sensor satellite observations. *Geophysical Research Letters* 37. <https://doi.org/10.1029/2009GL041828>
- Floutsi, A.A., Korras Carraca, M.B., Matsoukas, C., Hatzianastassiou, N., Biskos, G., 2019. The regime of Aerosol Optical Depth and Ångström exponent over Central and South Asia. *E3S Web of Conferences* 99, 2–6. <https://doi.org/10.1051/e3sconf/20199901003>
- Gaybullaev, B., Chen, S.-C., Gaybullaev, D., 2012. Changes in water volume of the Aral Sea after 1960. *Applied Water Science* 2, 285–291. <https://doi.org/10.1007/s13201-012-0048-z>
- Ge, Y., Abuduwaili, J., Ma, L., Liu, D., 2016. Temporal Variability and Potential Diffusion Characteristics of Dust Aerosol Originating from the Aral Sea Basin, Central Asia. *Water, Air, and Soil Pollution* 227. <https://doi.org/10.1007/s11270-016-2758-6>
- Groll, M., Opp, C., Aslanov, I., 2013. Spatial and temporal distribution of the dust deposition in central asia - results from a long term monitoring program. *Aeolian Research* 9, 49–62. <https://doi.org/10.1016/j.aeolia.2012.08.002>

Groll, M., Opp, C., Issanova, G., Vereshagina, N., Semenov, O., 2019. Physical and Chemical Characterization of Dust Deposited in the Turan Lowland (Central Asia). E3S Web of Conferences 99, 03005. <https://doi.org/10.1051/e3sconf/20199903005>

Hsu, N.C., Jeong, M.J., Bettenhausen, C., Sayer, A.M., Hansell, R., Seftor, C.S., Huang, J., Tsay, S.C., 2013. Enhanced Deep Blue aerosol retrieval algorithm: The second generation. Journal of Geophysical Research Atmospheres 118, 9296–9315. <https://doi.org/10.1002/jgrd.50712>

Hsu, N.C., Tsay, S.C., King, M.D., Herman, J.R., 2006. Deep Blue retrievals of Asian aerosol properties during ACE-Asia. IEEE Transactions on Geoscience and Remote Sensing 44, 3180–3195. <https://doi.org/10.1109/TGRS.2006.879540>

Hsu, N.C., Tsay, S.C., King, M.D., Herman, J.R., 2004. Aerosol properties over bright-reflecting source regions. IEEE Transactions on Geoscience and Remote Sensing 42, 557–569. <https://doi.org/10.1109/TGRS.2004.824067>

Huang, J., Lin, B., Minnis, P., Wang, T., Wang, X., Hu, Y., Yi, Y., Ayers, J.K., 2006. Satellite-based assessment of possible dust aerosols semi-direct effect on cloud water path over East Asia. Geophysical Research Letters 33. <https://doi.org/10.1029/2006GL026561>

Huang, J., Wang, T., Wang, W., Li, Z., Yan, H., 2014. Climate effects of dust aerosols over east asian arid and semiarid regions. <https://doi.org/10.1002/2014JD021796>

Issanova, G., Abuduwaili, J., Galayeva, O., Semenov, O., Bazarbayeva, T., 2015. Aeolian transportation of sand and dust in the Aral Sea region. International Journal of Environmental Science and Technology 12, 3213–3224. <https://doi.org/10.1007/s13762-015-0753-x>

Jin, Q., Wei, J., Yang, Z.L., Lin, P., 2017. Irrigation-induced environmental changes around the Aral Sea: An integrated view from multiple satellite observations. <https://doi.org/10.3390/rs9090900>

Kang, N., Raghavendra Kumar, K., Yin, Y., Diao, Y., Yu, X., 2015. Correlation Analysis between AOD and Cloud Parameters to Study Their Relationship over China Using MODIS Data (2003-2013): Impact on Cloud Formation and Climate Change. Aerosol and Air Quality Research 15, 958–973. <https://doi.org/10.4209/aaqr.2014.08.0168>

Kendall, M.G., 1975. Rank correlation methods. Griffin, London.

Levy, R., Hsu, C., Sayer, A., Mattoo, S., Lee, J., 2017. MODIS Atmosphere L2 Aerosol Product. NASA MODIS Adaptive Processing System, Goddard Space Flight Center. https://doi.org/10.5067/MODIS/MOD04_L2.061;10.5067/MODIS/MYD04_L2.061

Li, J., Carlson, B.E., Dubovik, O., Lacis, A.A., 2014. Recent trends in aerosol optical properties derived from AERONET measurements. *Atmospheric Chemistry and Physics* 14, 12271–12289. <https://doi.org/10.5194/acp-14-12271-2014>

Li, L., Sokolik, I.N., 2018. Analysis of dust aerosol retrievals using satellite data in Central Asia. *Atmosphere* 9. <https://doi.org/10.3390/atmos9080288>

Micklin, P., 2007. The Aral Sea Disaster. *Annual Review of Earth and Planetary Sciences* 35, 47–72. <https://doi.org/10.1146/annurev.earth.35.031306.140120>

MODIS Geolocation Fields 5-Min L1A Swath 1km V006, 2012.. MODIS Characterization Support Team, Level 1; Atmosphere Archive; Distribution System (LAADS). <https://doi.org/10.5067/MODIS/MOD03.006;10.5067/MODIS/MYD03.006>

Moosmüller, H., Engelbrecht, J.P., Skiba, M., Frey, G., Chakrabarty, R.K., Arnott, W.P., 2012. Single scattering albedo of fine mineral dust aerosols controlled by iron concentration. *Journal of Geophysical Research Atmospheres* 117. <https://doi.org/10.1029/2011JD016909>

Opp, C., Groll, M., Semenov, O., Vereshagina, N., Khamzina, A., 2019. Impact of the Aral Sea Syndrome - the Aralkum as a Man-Made Dust Source. *E3S Web of Conferences* 99, 03003. <https://doi.org/10.1051/e3sconf/20199903003>

Platnick, S.E., Ackerman, S.A., King, M.D., Meyer, K., Menzel, P., Frey, R., Holz, R., Baum, B., Yang, P., 2017. MODIS atmosphere L2 cloud product (06_L2). NASA MODIS Adaptive Processing System, Goddard Space Flight Center. https://doi.org/10.5067/MODIS/MOD06_L2.061;10.5067/MODIS/MYD06_L2.061

Platnick, S., King, M.D., Ackerman, S.A., Menzel, W.P., Baum, B.A., Riédi, J.C., Frey, R.A., 2003. The MODIS cloud products: Algorithms and examples from terra. *IEEE Transactions on Geoscience and Remote Sensing* 41, 459–472. <https://doi.org/10.1109/TGRS.2002.808301>

Rosenfeld, D., Andreae, M.O., Asmi, A., Chin, M., De Leeuw, G., Donovan, D.P., Kahn, R., Kinne, S., Kivekäs, N., Kulmala, M., Lau, W., Schmidt, K.S., Suni, T., Wagner, T., Wild, M., Quaas, J., 2014. Global observations of aerosol-cloud-precipitation-climate interactions. <https://doi.org/10.1002/2013RG000441>

Rosenfeld, D., Rudich, Y., Lahav, R., 2001. Desert dust suppressing precipitation: A possible desertification feedback loop. *Proceedings of the National Academy of Sciences of the United States of America* 98, 5975–5980. <https://doi.org/10.1073/pnas.101122798>

Rupakheti, D., Kang, S., Bilal, M., Gong, J., Xia, X., Cong, Z., 2019. Aerosol optical depth climatology over Central Asian countries based on Aqua-MODIS Collection 6.1 data: Aerosol variations and sources.

Atmospheric Environment 207, 205–214. <https://doi.org/10.1016/j.atmosenv.2019.03.020>

Sayer, A.M., Hsu, N.C., Bettenhausen, C., Jeong, M.J., 2013. Validation and uncertainty estimates for MODIS Collection 6 "deep Blue" aerosol data. Journal of Geophysical Research Atmospheres 118, 7864–7872. <https://doi.org/10.1002/jgrd.50600>

Sharif, F., Alam, K., Afsar, S., 2015. Spatio-Temporal distribution of aerosol and cloud properties over Sindh using MODIS satellite data and a HYSPLIT model. Aerosol and Air Quality Research 15, 657–672. <https://doi.org/10.4209/aaqr.2014.09.0200>

Shen, H., Abduwaili, J., Ma, L., Samat, A., 2019. Remote sensing-based land surface change identification and prediction in the Aral Sea bed, Central Asia. International Journal of Environmental Science and Technology 16, 2031–2046. <https://doi.org/10.1007/s13762-018-1801-0>

Shen, H., Abduwaili, J., Samat, A., Ma, L., 2016. A review on the research of modern aeolian dust in Central Asia. Arabian Journal of Geosciences 9. <https://doi.org/10.1007/s12517-016-2646-9>

Soni, K., Singh, S., Bano, T., Tanwar, R.S., Nath, S., 2011. Wavelength dependence of the aerosol Angstrom exponent and its implications over Delhi, India. Aerosol Science and Technology 45, 1488–1498. <https://doi.org/10.1080/02786826.2011.601774>

Spearman, C., 1987. The proof and measurement of association between two things. By C. Spearman, 1904. The American journal of psychology 100, 441–471. <https://doi.org/10.2307/1422689>

Stephens, G.L., Paltridge, G.W., Platt, C.M.R., 1978. Radiation Profiles in Extended Water Clouds. III: Observations. [https://doi.org/10.1175/1520-0469\(1978\)035<2133:rpiewc>2.0.co;2](https://doi.org/10.1175/1520-0469(1978)035<2133:rpiewc>2.0.co;2)

Wood, R., 2006. Relationships between optical depth, liquid water path, droplet concentration and effective radius in an adiabatic layer cloud. University of Washington report, 2–4. https://doi.org/https://atmos.uw.edu/~robwood/papers/chilean_plume/optical_depth_relations.pdf

Yin, X.M., Dai, T., Xin, J.Y., Gong, D.Y., Yang, J., Teruyuki, N., Shi, G.Y., 2016. Estimation of aerosol properties over the Chinese desert region with MODIS AOD assimilation in a global model. Advances in Climate Change Research 7, 90–98. <https://doi.org/10.1016/j.accre.2016.04.001>

Yin, Y., Wurzler, S., Levin, Z., Reisin, T.G., 2002. Interactions of mineral dust particles and clouds: Effects on precipitation and cloud optical properties. Journal of Geophysical Research Atmospheres 107. <https://doi.org/10.1029/2001JD001544>

7 Appendix

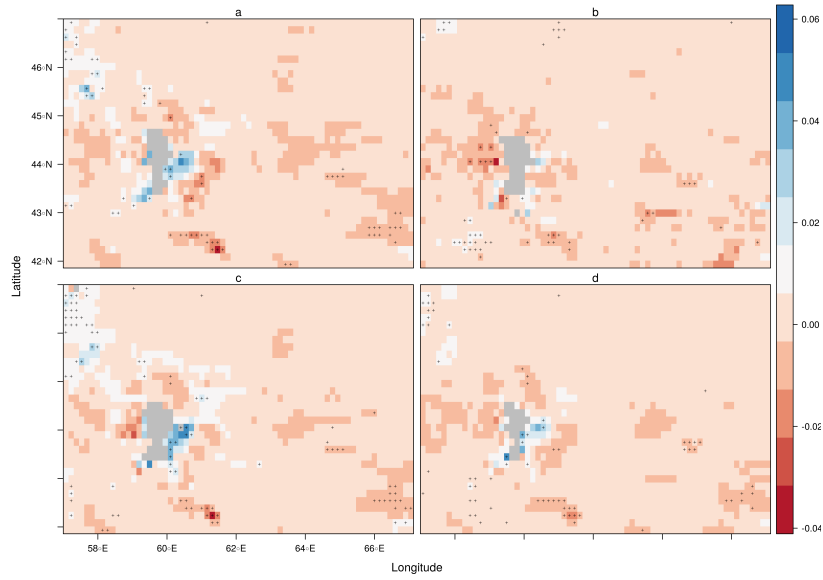


Figure 17: Spatial distribution of linear trend for AOD during spring (a), summer (b), autumn (c), and winter (d).

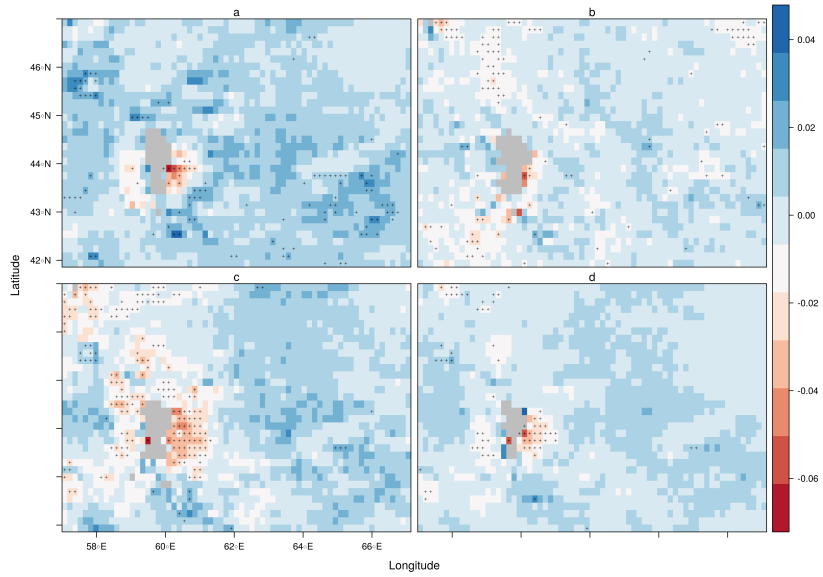


Figure 18: Spatial distribution of linear trend for AE during spring (a), summer (b), autumn (c), and winter (d).

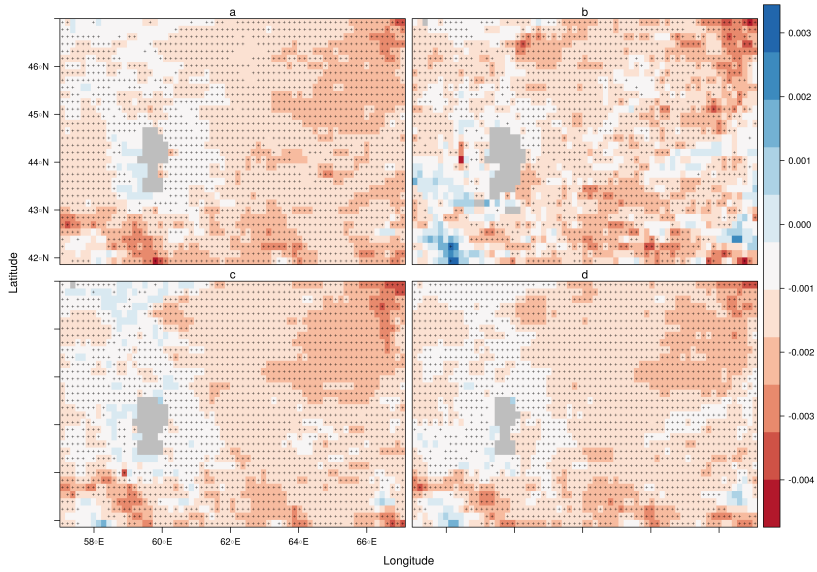


Figure 19: Spatial distribution of linear trend for SSA during spring (a), summer (b), autumn (c), and winter (d).

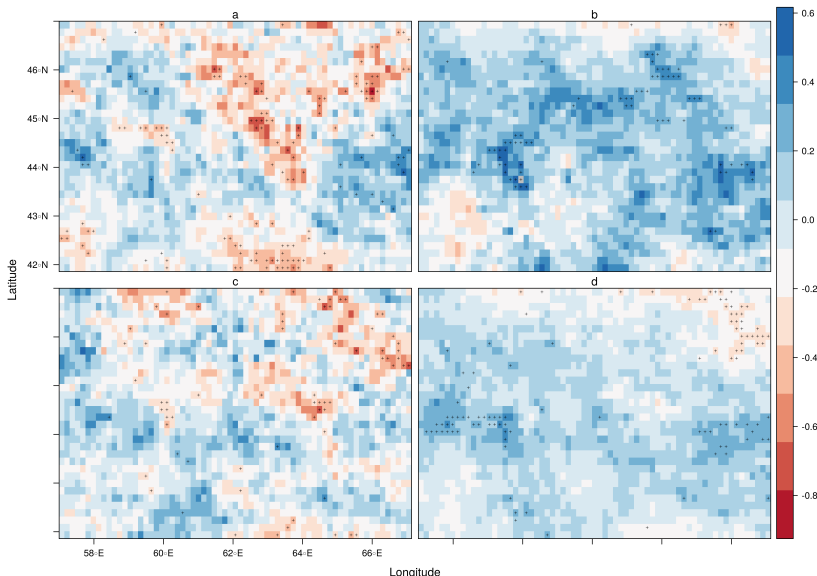


Figure 20: Spatial distribution of linear trend for COT during spring (a), summer (b), autumn (c), and winter (d).

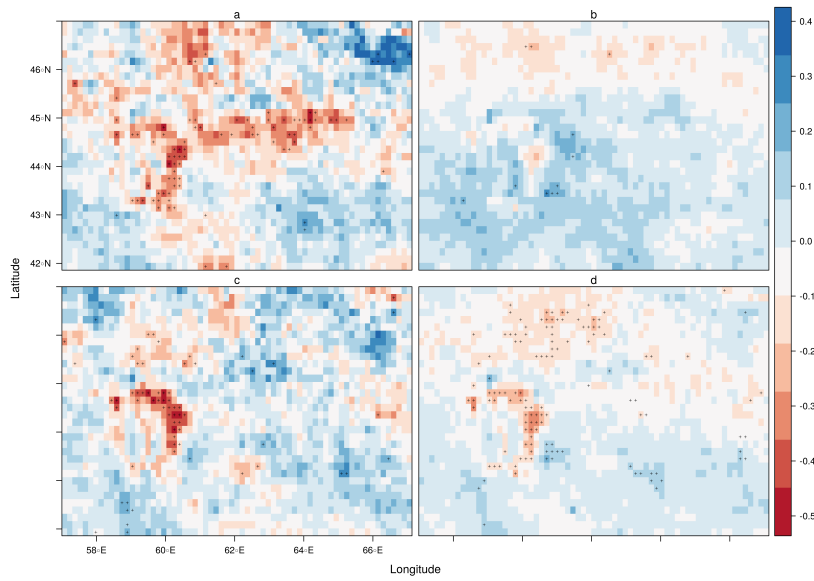


Figure 21: Spatial distribution of linear trend for CER [in microns] during spring (a), summer (b), autumn (c), and winter (d).

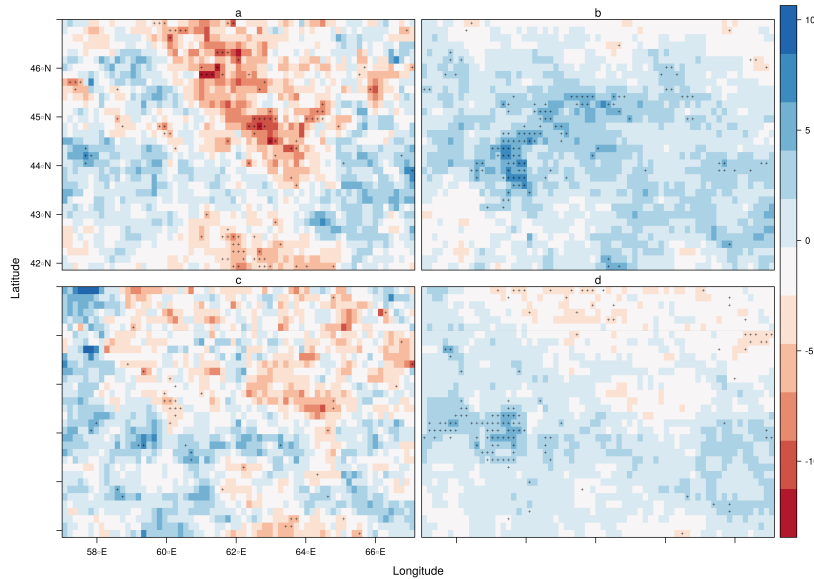


Figure 22: Spatial distribution of linear trend for CWP [in g/m²] during spring (a), summer (b), autumn (c), and winter (d).